Journal of Fundamental and Applied Sciences

Research Article

ISSN 1112-9867

Available online at http://www.jfas.info

ELECTROCHEMICAL AND THEORETICAL STUDIES INFLUENCING THE EFFECT OF HYDROXYL POSITION OF TETRAPHENOLIC SCHIFF BASES TOWARDS CORROSION INHIBITION OF MILD STEEL IN 1M HCl

A. Kheniche[1,2*], A. Ourari[1], A. Dakhouche[2], A. Ghanem[2], W. Min[3], K. Meguellati[3]

[1]Laboratoire d'Electrochimie, d'Ingénierie Moléculaire et de Catalyse Redox (LEIMCR), Faculté de Technologie, Université Ferhat ABBAS Sétif-1, 19000, Algeria

[2]Laboratoire des matériaux inorganiques (LMI), Université de M'sila 28003, Algeria

[3]International Joint Research Laboratory of Nano-MicroArchitecture Chemistry, College of Chemistry, Jilin University, 2699 Qianjin Street, Changchun 130012, P. R. China

Received: 02 February 2018 / Accepted: 10 June 2018 / Published online: 01 September 2018

ABSTRACT

The effect of three tetrahydroxylated Schiff bases as *N*,*N*-bis(2,3-dihydroxybenzyl-idene)-4,4'-diphenylmethane, *N*,*N*-bis(2,4-dihydroxybenzyl- idene)-4,4'-diphenylmethane and *N*,N-bis(2,4-dihydroxybenzylidene)-4,4'-diphenylmethane were studied as inhibitors for mild steel in 1M HCl medium. The experiments were performed using potentiodynamic polarization. This inhibition proved an efficient increase according the position of second hydroxyl of salicylaldehyde suggesting that this inhibition is dependent on concentration and the compound nature. Among these position-isomers, the best inhibition efficiency was obtained with p-hydroxylated (94%) at 1mM. Tafel plots of these inhibitors are the mixed-type, their adsorption is spontaneous obeying to Langmuir's isotherm. AFM/SEM-EDS characterized metal surface. DFT-calculations and molecular dynamics simulations are correlated to inhibition efficiency obtained.

Keywords: Mild steel, Tetrahydroxylated H_2Salen, Corrosion inhibitors, AFM and SEM images, DFT-calculations and molecular dynamic simulations.

Author Correspondence, e-mail: hakiche2000@yahoo.fr

doi: http://dx.doi.org/10.4314/jfas.v10i3.16

1. INTRODUCTION

Mild steel is known as the most important element in construction materials, and has been broadly employed in chemical industries, but is sensitive to the aggressive solutions. Hydrochloric acid has widespread uses in the acidic pickling of steel and ferrous alloys, acid rescaling, acid cleaning and oil well cleaning [1–2]. Hence, assiduous attempts have been employed on needs to promote and design efficient corrosion inhibitors that prevent corrosion. The need of reducing corrosion process requires the use of inhibitors, especially organic compounds that represent the straightforward ways for avoiding corrosion under acidic media [3–5]. Overall, the heterogeneous organic compounds possess polar character caused by heteroatoms such as nitrogen, oxygen and Sulphur having a tendency to resist against corrosions, which are considered as the efficient adsorption centers to their chemical structure and can create a stable chelate with metals [6–8]. Therefore, the adsorption of these molecules with their size, orientation, shape and electric charge could influence seriously the performances of these inhibitors against the corrosion [19–21].

Schiff bases are the result of condensation of amine and carbonyl compounds, which were found to have several applications as active molecules in pharmaceutical, biological and industrial fields [11–14]. Debates, involving corrosion inhibition in recent years, confirmed that Schiff bases are efficient as corrosion inhibitors under different corrosive media [15–17]. So, the inhibitive activity of three phenolic Schiff bases have been tested towards the resistance of mild steel against corrosion in presence of in 0.5 M HCl solution. This led to 97% as exhibition of hindrance efficiency [18]. Newly, two phenolic Schiff bases (A) and (B), in which (B) is substituted in para position by bromine whereas (A) with hydrogen, have been evaluated for corrosion of C1018 steel in aggressive environment 2 M HCl. The findings supported by molecular dynamic simulation proved that the inhibition performance of Schiff base (B) > Schiff base (A) [19]. Elsewhere, the effect of hydroxyl group position on corrosion hindrance of Schiff bases has been examined on steel electrode in 1 M HCl by using electrochemical techniques and quantum calculations [20]. The outcomes denote that IE% is extremely linked to some quantum parameters except with different degrees. It is worth noting that, the uses of the quantum chemical approach is gradually becoming more significant to

predict the relation chip between electronic properties and the anticorrosive activity of preventive molecules [21–23]. The huge significance of dynamic molecular simulations is to uncover the stable spatial orientation of inhibitor during the adsorption process on the metal surface, and consequently determine the adsorption energy value [24–26].

In the present research, we have synthesized three tetraphenolic Schiff bases, namely, N,N-bis(2,3-dihydroxybenzylidene)-4,4'-diphenylmethane (2,3-DHDPMM), N,N-bis(2,4-dihydroxybenzylidene)-4,4'-diphenylmethane (2,4-DHDPMM) and N,N-bis(2,5-dihydroxybenzylidene)-4,4'-diphenylmethane (2,5-DHDPMM). Their molecular structures are below illustrated in Fig.1:

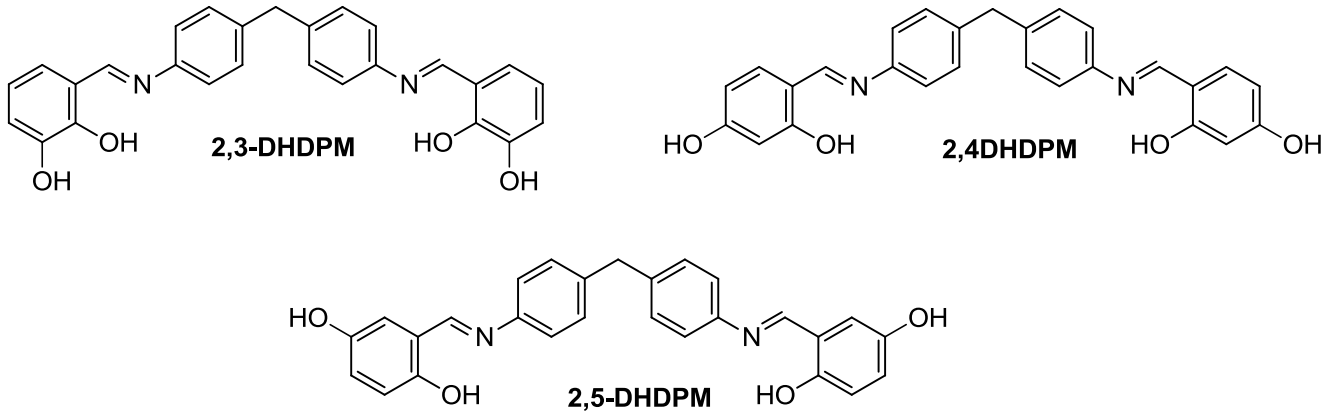

Fig.1. Chemical structures of the tested Schiff bases

The structural choice of these compounds is supported by covering three other positions like 3,4 and 5 for the second hydroxyl group in the salicylaldehyde moieties. In addition, the presence of four hydroxyl groups on the aromatic moieties produce at least two probable protonated sites causing an increasing in the adsorption of these molecules on metal surface. Moreover, this study draws to prior research that based on the continuation of our works like those early reported by N. Belhadj *et al*. [27] and L. Toukal *et al*. [28]. The corrosion inhibition measurements were achieved on mild steel in 1 M HCl solution through electrochemical techniques such as potentiodynamic polarization and impedance spectroscopy (EIS). The surface exploration was carried out using scanning electron microscopy (SEM) and atomic force microscopy analysis (AFM). Thermodynamic parameters and adsorption isotherms of

inhibitors on the mild steel surface was achieved. However, the theoretical modelling via Density Functional Theory (DFT) and molecular dynamic simulations approach was also applied to corroborate between electronic and molecular structures and IE%.

2. RESULTS AND DISCUSSION

2. 1. Potentiodynamic polarization measurements

The responses of the potentiodynamic polarization curves of X52 in HCl (1M) with and without inhibitors are shown in Fig. 2. Corrosion potential (E_{corr}), corrosion current density (I_{corr}), anodic Tafel slope (βa) and cathodic Tafel slope (β_C), and inhibition efficiency (*IE%*) were deducted from the curves and are listed in Table 1**.** Table 1 provides evidence of the potential corrosion shift towards the anodic region [29]. According to the literature, if a shift of E_{corr} is higher than 85 mV (E_{corr}vs. ESC), the inhibitor could be considered as cathodic or anodic, and if the shift of (E_{corr}vs. ESC) is lower than 85 mV, the inhibitor can working as a mixed type. From our studies, the largest shift compared with the blank was 20 mV suggesting that the inhibitor is also a mixed-type. Consequently, these inhibitors can be identified as mixed forms that can delay the release of dihydrogen in the cathodic reaction and inhibiting the anodic dissolution of MS. This behaviour was emphasized by adsorption of the studied inhibitors on the surface of metal, which induces an energetic barrier linked to the mass and the charge density for the anodic and cathodic reactions [30]. The lowest values of I_{corr} were observed in the existence of ligands (SBs) 82.29; 91.43 and 43.82 µA.cm^{-2} for 1 mmol of 2,3-DHDPM, 2,4-DHDPM and 2,5-DHDPM, respectively. Inhibition efficiency (IE %) was increased by increasing the concentration of the inhibitors.

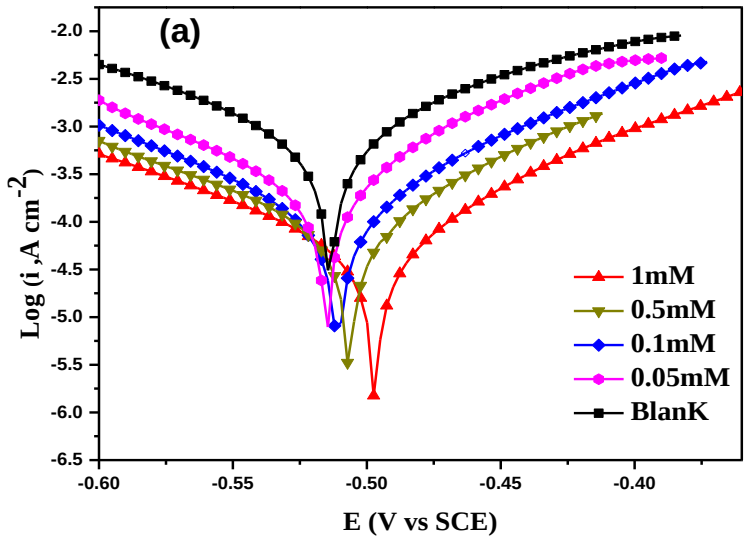

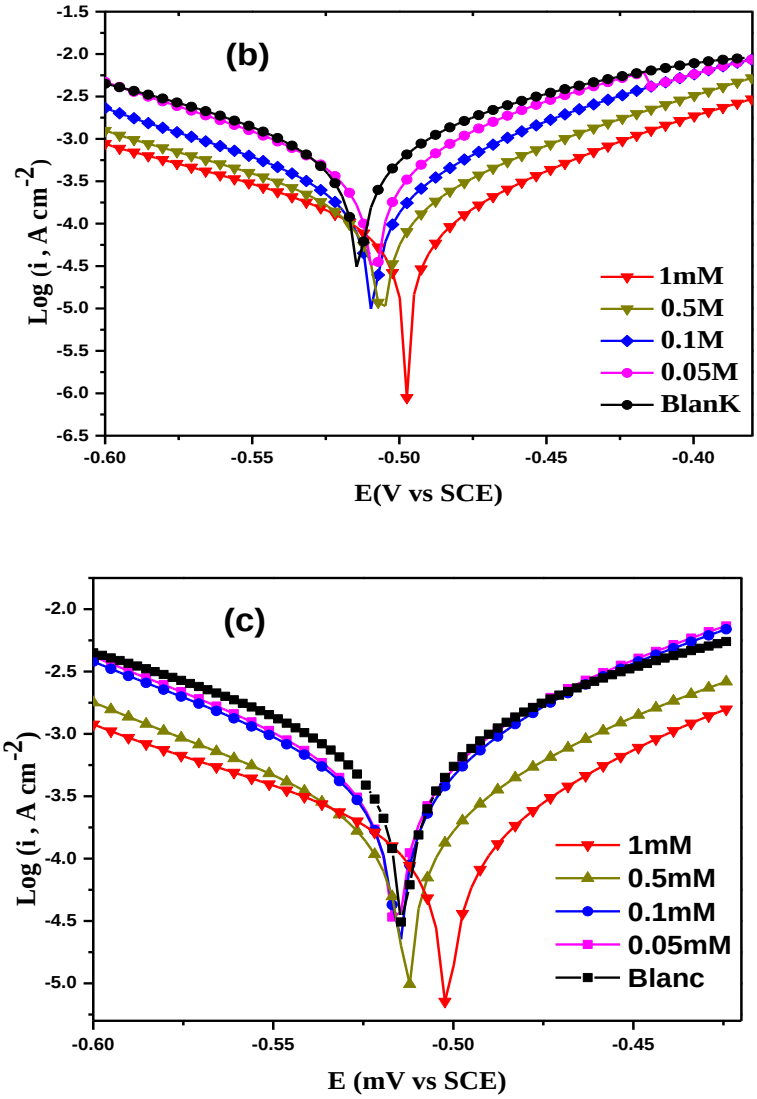

Fig.2. Polarization curves for mild steel in 1 M HCl in the presence of Schiff bases at different concentrations (a) 2,5-DHDPM, (b) 2,3-DHDPM, (c)) 2,4-DHDPM

The largest value of inhibition efficiency (IE %) was estimated to be 88.17% for an optimal concentration of 1 mmol of inhibitor **2**,5-DHDPMM. Thus, the results indicated that the percentage of inhibition efficiency of 2,5-DHDPMM is higher than those of all other inhibitors. The largest value of inhibition efficiency (IE %) was estimated to be 88.17% for an optimal concentration of 1 mmol of inhibitor 2,5-DHDPMM. Thus, the results indicated that the percentage of inhibition efficiency of 2,5-DHDPMM is higher than those of all other inhibitors.

The values of the slope of the cathodic (βc) and anodic (βc) Tafel lines are slightly changed by

increasing the concentration of the studied compounds. This denotes that the hydrogen release process is dominated by activation.

These outcomes exhibit that moving the hydroxyl group to the ortho position (2,4-DHDPM) prompted a decrease in its ability to be adsorbed leading to 75.30% as inhibition efficiency. Nevertheless, when moving to the para position, the implicated compound like (2,5-DHDPM) provokes a significant increase in the inhibition efficiency attaining 88.11%. A simple correlation of the 2,5-DHDPM and 2,4-DHDPM inhibition efficiencies (88.11% versus 75.3%) uncovers that this effect of the substituent position evidently improved the co-planarity of different sp2-moeities of the molecule rendering it easily adsorbed.

Table 1. Electrochemical corrosion parameters for mild steel in 1 M HCl in the absence and presence of Schiff bases at various concentrations

compounds	C(M)	E_{corr} (mV/SCE)	I_{corr} (μA/cm²)	-bc (mV/dec)	Ba (mV/dec)	η%	θ
Blank	-	-516.3	370.18	58.251	60.38	-	-
	1	-495.9	43.8	62.8	42.0	88,2	0.88
	0.5	-508. 6	143.0	64.6	51.7	61,4	0.61
2,5-DHDPM	0.1	-467.0	175.8	57.8	53.8	53,0	0.53
	0.05	-509.5	277.7	80.1	108.5	25,2	0.25
	1	-499.6	82.3	83.1	67.8	78,0	0.78
	0.5	-508.4	143.9	71.7	49.2	61,1	0.61
2,3-DHDPM	0.1	-515.3	205.0	60.7	47.7	44,6	0.45
	0.05	-517.7	290.2	56.3	48.2	21,6	0.22
	1	-504.3	91.4	71.6	60.5	75,3	0.75
	0.5	-514.6	155.8	53.6	53.0	57,9	0.58
2,4-DHDPM	0.1	-514.9	255.9	47.9	62.0	30,9	0.31
	0.05	-516.1	293.2	62.4	51.1	20,8	0.21

2.2. Adsorption isotherms

The adsorption isotherms can give favourable interpretation for the mechanism of corrosion prevention. Some attempts were performed to adapt surface cover (θ, expressed in IE % / 100) to the different isotherms including those of Frumkin, Langmuir and Temkin models. By far, the best adjustment was obtained for the Langmuir adsorption represented in Fig. 3.

According the following equation 1:

$$\frac{C_{inh}}{\theta} = \frac{1}{K} + C_{inh} \quad (1)$$

Where C_{inh} is the concentration of inhibitor and K is the adsorption equilibrium constant. Fig. 3 displays the adsorption curve of the studied ligands (SBs) on the surface of MS with its relationship between $\frac{C_{inh}}{\theta}$ and C_{inh} at 30°C.

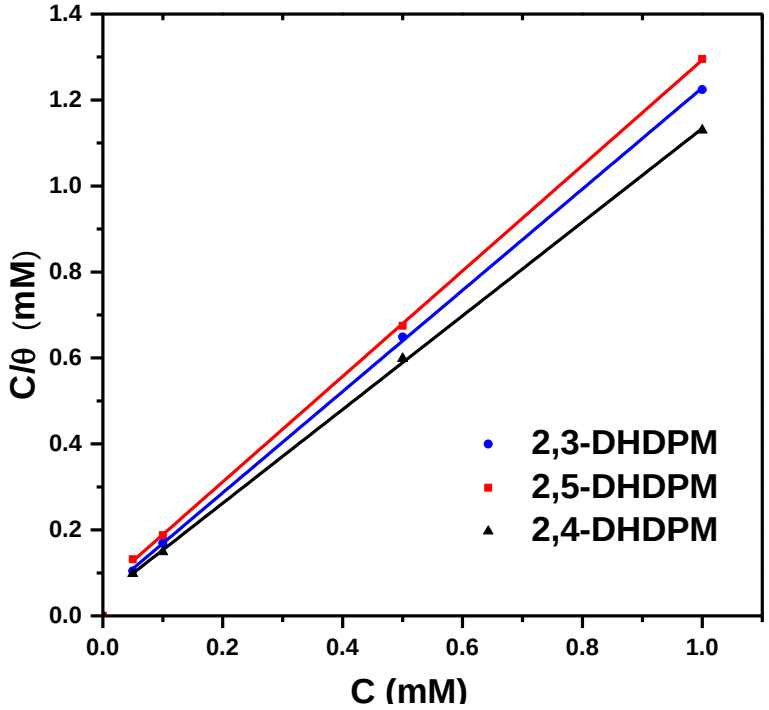

Fig.3. Langmuir isotherm for adsorption of Schiff bases on the steel surface

Table 2. Adsorption parameters for 2,3-DHDPM, 2,4-DHDPM and 2,5-DHDPM calculated from Langmuir isotherm for mild steel in an aqueous solution of 1M HCl at 303 K

	ΔG_{ads} (kJ.mol^{-1})	K_{ads} (M^{-1})	R^2
2,3-DHDPM	-35.00	19607.84	0.9998
2,4-DHDPM	-34.35	15082.95	0.9999
2,5-DHDPM	-35.37	22573.36	0.9997

Gibbs free energy (ΔG_{ads}) was calculated according to the following equation 2 [31]:

$$\Delta G^0_{ads} = -RTLn(55.55K) \quad (2)$$

Where *R* is the universal gas constant, *T* is the absolute temperature in *K*, and the numerical value 55.5 represents the molar concentration of water in the acid solution. Generally, a high

value of K_{ads} is associated with high adsorption efficiency. In our present case, the values of K_{ads} follow the order 2,4-DHDPM < 2,3-DHDPM < 2,5-DHDPM, which is consistent with the order of the inhibition efficiency. The negative values of ΔG^0_{ads} given in Table 2 suggests that the ligands (SBs) are spontaneously adsorbed on the MS surface [32,33]. In the present work, the values of ΔG^0_{ads} were found to be between -34.35 and -35.37 kJ mol^{-1}, implying that the adsorption protocol occurs according physisorption mechanism [34].

An important enrichment in electron density around the heteroatoms N of (-C=N-), O of (-OH-) and the aromatic rings of our ligands (SBs) have induced the highest inhibitory efficiency for these compounds. As consequence, the adsorption of inhibitors on the surface of the electrode can be explained by assuming donor-acceptor interactions between π–electrons of the aromatic rings of inhibitors and vacant d-orbitals on the surface of Fe atoms [35]. Furthermore, the adsorption of ligands (SBs) on the MS surface is due to the presence of phenolic and imine groups. Among the studied SBs, 2,5-DHDPM is the molecule which have given the highest inhibitory efficiency compared to the others: 2,3-DHDPM and 2,4-DHDPM. The effectiveness of para-position of the hydroxyl group (-OH) of the inhibitor 2,5-DHDPM can be attributed to the planarity of the molecule, which makes it more rigid and increases its adsorption ability to the metal. Additional details can be obtained from the quantum study.

2.3 Effect of temperature

Temperature effect was evaluated at diverse temperatures (303-333K) in the absence or presences of optimum concentration of inhibitor. The thermodynamic parameters of the corrosion process were estimated by using Arrhenius equation 3 and the transition state equation 4 of its intermediate as follows:

$$i_{corr} = K \exp\left(\frac{-E_a}{RT}\right) \quad (3)$$

$$K = \frac{RT}{Nh}\exp\left(\frac{\Delta S^*}{R}\right)\exp\left(\frac{\Delta H^*}{RT}\right) \quad (4)$$

where i_{corr} refers to the corrosion current density, E_a is the activation energy, T is the temperature, h is the Planck constant, N is the Avogadro constant, ΔS^* is the entropy of activation and ΔH^* is the enthalpy of activation .

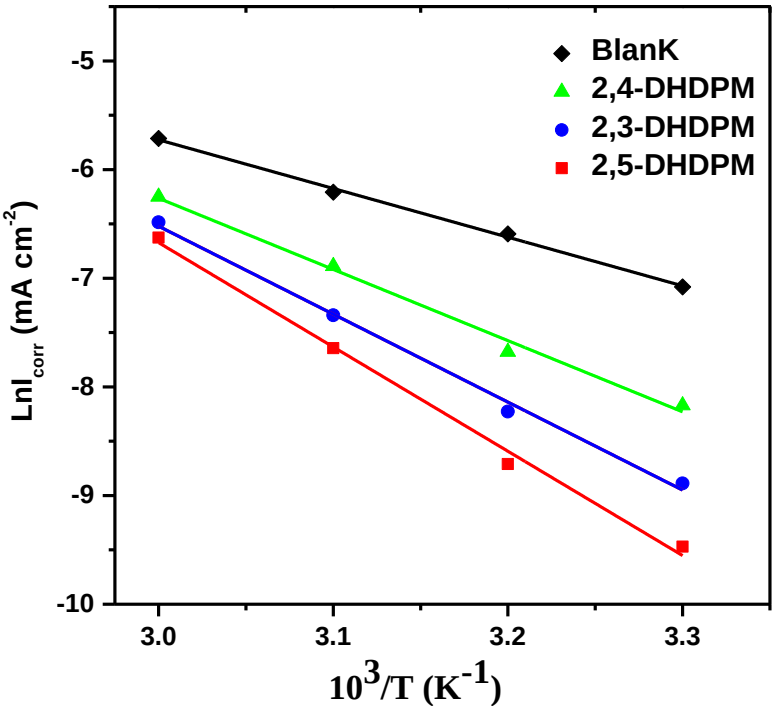

Fig.4. Arrhenius plots of ln(Icorr) vs. 1/T for X52 in 1 M HCl in the absence and presence of 1 mM of different inhibitors

As shown in Fig. 4, the energy of activation and pre-exponential factors were calculated from the linear regression of Ln (i_{corr}) vs *1/T* where *T* corresponds to the studied temperature, their data are gathered in Table 3. In fact, the inhibitory efficiency decreased with temperature, which accelerated the corrosion process, and triggered the dissolution of the metal and mediated the shift of equilibrium to desorption.

Table 3. Activation parameters E_a,, ΔH* and ΔS* of the dissolution of X52 in 1M HCl in presence of inhibitor

.	Ea (kJ.mol^{-1})	ΔH (kJ.mol^{-1})	ΔS (J.mol^{-1}.K^{-1})
Blank	33.25	6.48	-175.34
2,3-DHDPM	67.34	14.96	-152.14
2,4-DHDPM	54.45	11.22	-162.45
2,5-DHDPM	79.81	18.62	-141.42

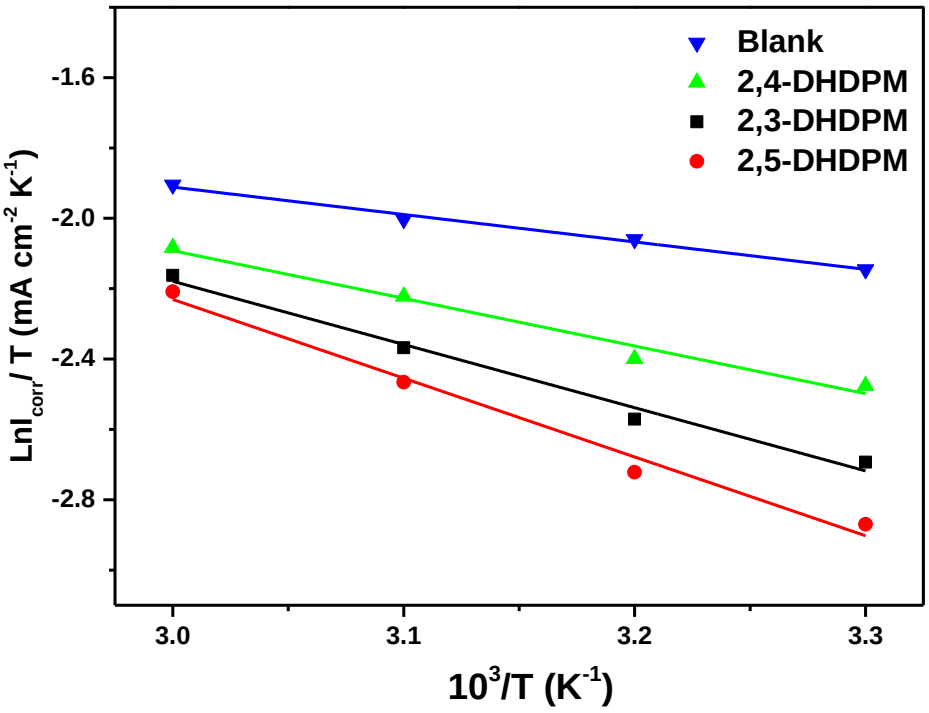

Fig.5. Alternative Arrhenius plots for mild steel in 1M HCl in the absence and presence of 1 mM of different inhibitors

The slopes of Fig. 5 (Curves A and B) exhibit the ratio of $\Delta H^* / R$ and the intercept gives the value of (ln (R/Nh) + $\Delta S^* / R$), from which ΔH^* and ΔS^* were calculated, as shown in Table 3. Positive enthalpy (ΔH^*) indicates the endothermal process of a complex dissolution process of MS. Negative values of ΔS^* denote that entropy decreases during the formation of the transition state, which frequently proves the associative mechanism leading to the formation of single complex [36].

2.4 Atomic Force microscopy studies

Atomic Force Microscopy is a technique allowing to characterize nanostructured materials [37,38]. Three-dimensional AFM images of the steel surface handled with 1 M HCl are illustrated in Fig. 6(b). As shown in Fig. 6(b), the corrosion of MS, in the absence of inhibitor, displayed an irregular surface area, indicating that the surface is highly corroded. The average rugosity (R_a) of MS in a 1 M HCl solution without an inhibitor was found to be equal to 584.1 nm. However, in the presence of inhibitor, the Fig. 6(c), Fig. 6(d) and Fig. 6(e) showed images of surfaces appearing as regular. Moreover, the calculated average surface roughness (R_a) were 49.8… 57.5 and 104.8 nm for 2,3-DHDPMM, 2,4-DHDPMM and 2,5-DHDPMM, respectively. The values of R_a of the tested inhibitors decreased causing less damage due to the formation of preventive layer of the inhibitor on the MS surface. Also, the recording of images of samples before and after immersion in 1 M HCL media are shown by the Fig. 7(a-e). This figure exhibits the analysis results of AFM with its two-dimensional images of X52 surface.

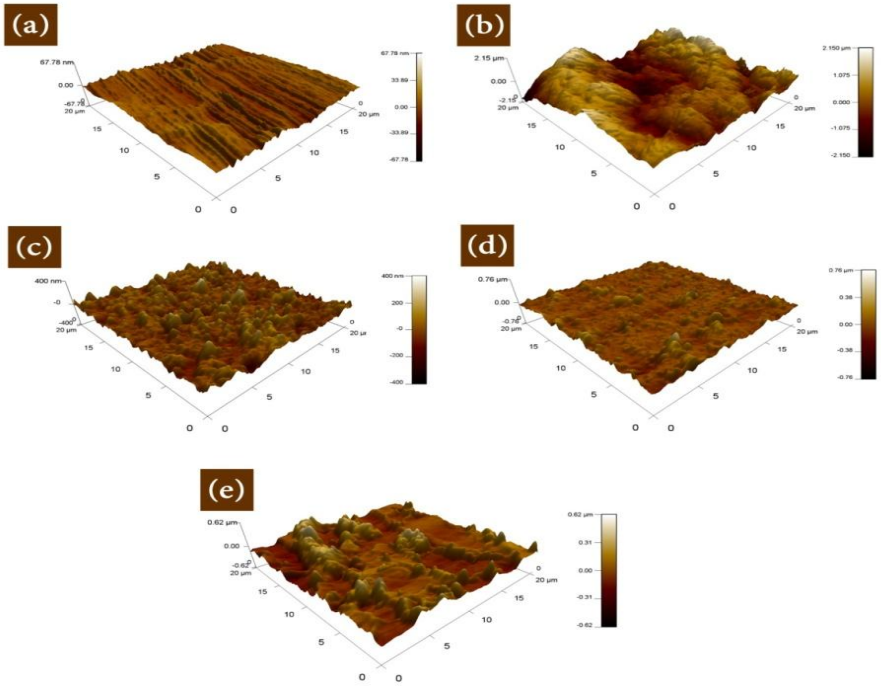

Fig.6. AFM three-dimensional images of X52 surface: before immersion (a); after immersion in 1.0 M HCl (b) ; 10^{-3}M 2,3-DHDPM with 1.0 M HCl (c); 10^{-3}M 2,4-DHDPM with 1.0 M HCl (d); 10^{-3}M 2,5-DHDPM with 1.0 M HCl (e) after 24 h of immersion at 20°C

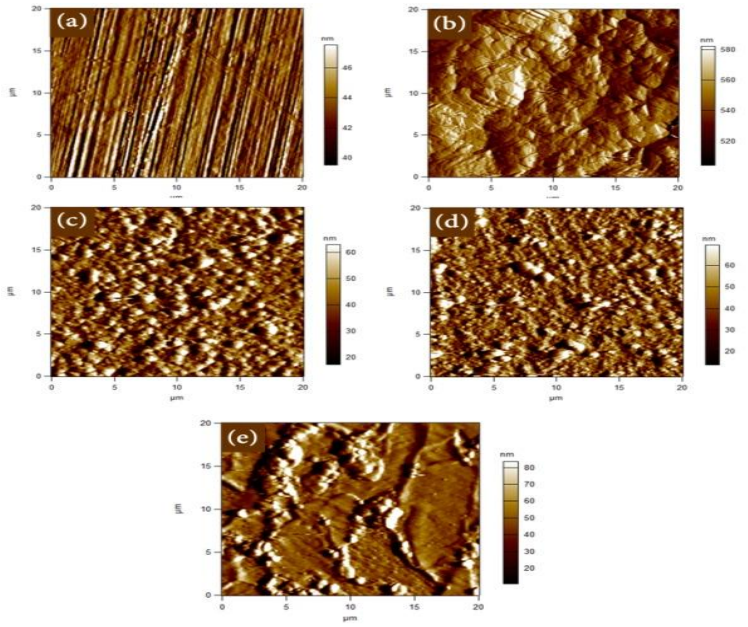

Fig.7. AFM two-dimensional images of X52 surface: before immersion (a); after immersion in 1.0 M HCl (b) ; 10^{-3}M 2,3-DHDPM with 1.0 M HCl (c); 10^{-3}M 2,4-DHDPM with 1.0 M HCl (d); 10^{-3}M 2,5-DHDPM with 1.0 M HCl (e) after 24 h of immersion at 20°C

2.5. SEM Analysis/ EDX examinations of electrode surface

The SEM is an useful technique for monitoring surface state and adsorption process during the corrosion of MS. Fig. 8(a), Fig. 8(b) and 8(c–e) represent the SEM micrographs of the X52 bare surface, CS specimens, in the presence and absence of the inhibitor in acidic solution, respectively. Fig. 8(a) shows that the surface of MS sample is very smooth and displayed no marks of corrosion. Unlike, the Fig. 8(b) which shows a damaged surface confirming its corrosion attack. Whereas, in the presence of ligands (SBs), the Fig. 8(c-e) presenting the specimens displaying less damages with smooth surface as a result of the formation of a protective layer of inhibitors (SBs). This indicates the prohibition of the dissolution of iron and consequently reduces the rate of corrosion of MS in 1.0 M HCl solution. The EDX profile analysis was carried out to identify the composition of the species formed on the metal surface in 1 M hydrochloric acid in the absence and presence of SBs. Fig. 9(a) represents EDX spectrum for abraded MS samples showing the distinctive peaks of the elements constituting MS sample. The EDX analysis of corroded sample showed that the surface film contains mostly Fe with little proportions of C, O and Cl as it can be seen in Fig. 9(b).

Furthermore, the appearance of new peak of nitrogen and oxygen in the adsorbed film confirm that SBs molecules were strongly adsorbed on the MS surface as illustrated by Fig. 9(c-e).

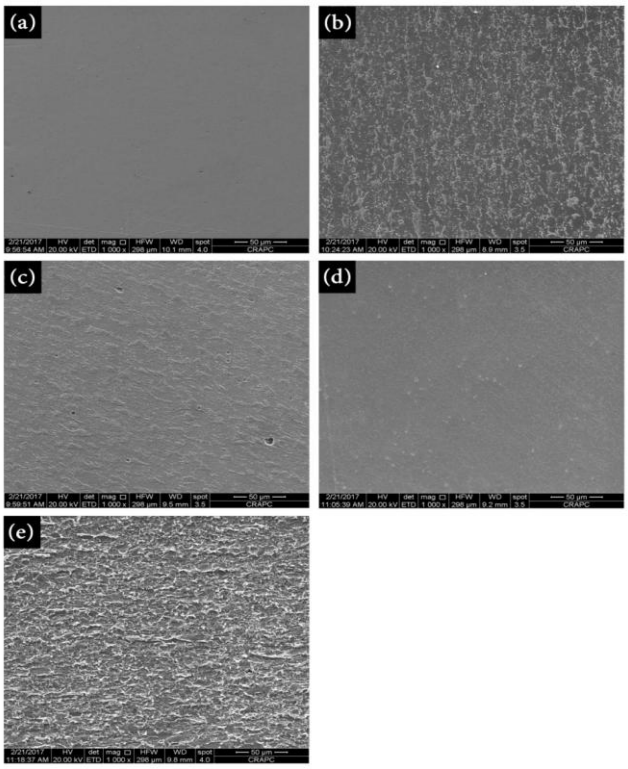

Fig.8. SEM images of X52 surface: before immersion (a); after immersion in 1.0 M HCl (b) ; 10^{-3}M 2,3-DHDPM + 1.0 M HCl (c); 10^{-3}M 2,4-DHDPM + 1.0 M HCl (d); 10^{-3}M 2,5-DHDPM + 1.0 M HCl (e) after 24 h of immersion at 20°C

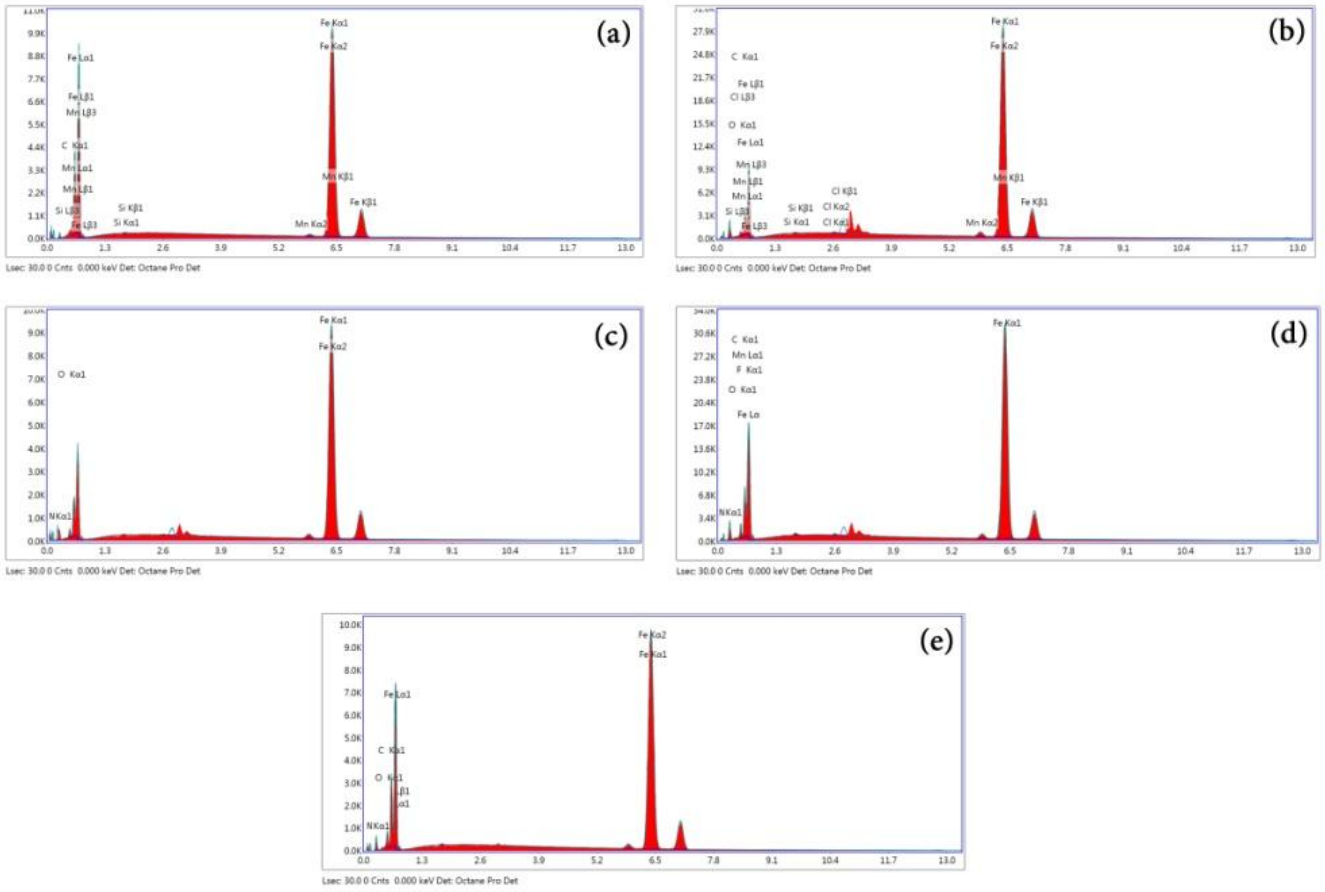

Fig.9. EDX spectra of MS (a), MS in 1 M HCl (b), MS in 1 M HCl with 2,3-DHDPM (c), MS in 1 M HCl with 2,4-DHDPM (d) and MS in 1 M HCl with 2,5-DHDPM (e) at 1mM

2.6. Theoretical calculations

In order to survey the mechanism of adsorption and inhibition, relating the molecular structure to the inhibitory capability, quantum chemical calculations were achieved with Gaussian 9 software. The experimental results proved that the inhibitory effects of 2,3-DHDPMM, 2,4-DHDPMM and 2,5-DHDPMM take place via a chemical adsorption mechanism. To improve the study of the electron interaction between inhibitory molecules and the MS surface, several theoretical parameters were investigated in the literature such as the energy of molecular orbitals (E_{HOMO}, E_{LUMO}) which were determined by optimization. So, the calculated quantum chemical parameters were ΔE, χ , β , σ and ΔN [39, 40] are collected in Table 4.

Table 4. Quantum chemical parameters calculated with DFT level using the 6-31g (d) basis set for 2,3-DHDPM, 2,4-DHDPM and 2,5-DHDPM

Inhibitor	E_{HOMO} (eV)	E_{LUMO} (eV)	ΔE (eV)	β (eV)	γ (eV)	s (eV^{-1})	ΔN	μ (Debye)
2,3-DHDPM	-5.4	-1.35	4.05	3.37	2.02	0.49	0.895	5.2
2,4-DHDPM	-5.28	-1.21	4.07	3.24	2.03	0.49	0.922	4.07
2,5-DHDPM	-5.36	-1.43	3.93	3.39	1.96	0.51	0.917	5.7

The frontier molecular orbital theory describes the E_{HOMO}/ E_{LUMO} interaction. A lower gap (ΔE) between E_{HOMO} and E_{LUMO} means an increase in interactions [41]. The following equations were employed for calculating quantum chemical parameters such as the absolute electronegativity parameter (χ), global hardness (η), the softness (σ) and the fraction of electrons transferred (ΔN) [42].

$$\chi = -\frac{E_{HOMO} + E_{LUMO}}{2} \quad (5)$$

$$\eta = \frac{E_{HOMO} - E_{LUMO}}{2} \quad (6)$$

$$\sigma = \frac{1}{\eta} \quad (7)$$

$$\Delta E = E_{LUMO} - E_{HOMO} \quad (8)$$

$$\Delta N = \frac{\chi_{Fe} - \chi_{Inh}}{2\left(\gamma_{Fe} + \gamma_{Inh}\right)} \quad (9)$$

It has previously been noticed that the lower values of ΔE are correlated with an increase in inhibitory potential [43]. A lower energy gap (Δ*E*) improves the yield of inhibition, as the energy necessary to remove one electron from the external orbital is minimized. Generally, strong acids have a higher affinity for strong bases and soft acids for soft bases. Iron is considered to be a soft acid and can be coordinated with the softer molecules for its lower energy gap (ΔE) to form a stable complex on the metal surface. The higher values of E_{HOMO} and the lower values for ΔE and E_{LUMO} are those of 2,5-DHDPMM compared to the corresponding values of 2,3-DHDPMM and 2,4-DHDPMM. This comparison concluded that

2,5-DHDPMM has greater capacity to combine to the surface of MS, suggesting its high efficiency as inhibitor. Figs. 10 and 11 showed the optimized geometry since, the HOMO and LUMO densities of distribution allowed to propose the mechanism governing the modes of diverse interactions between different molecular moieties including functional groups inducing the co-planarity of sp^2 entities associated to its electronic delocalization (See Fig. 10).

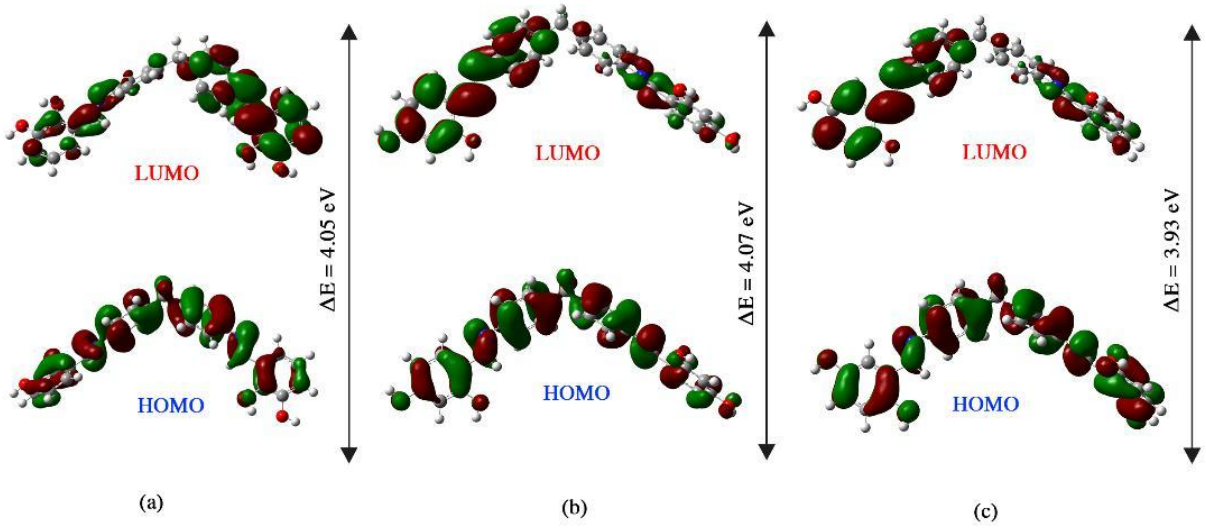

Fig.10. Frontier molecule orbital density distributions of: HOMO (a) and LUMO obtained from B3LYP/6-31G** method

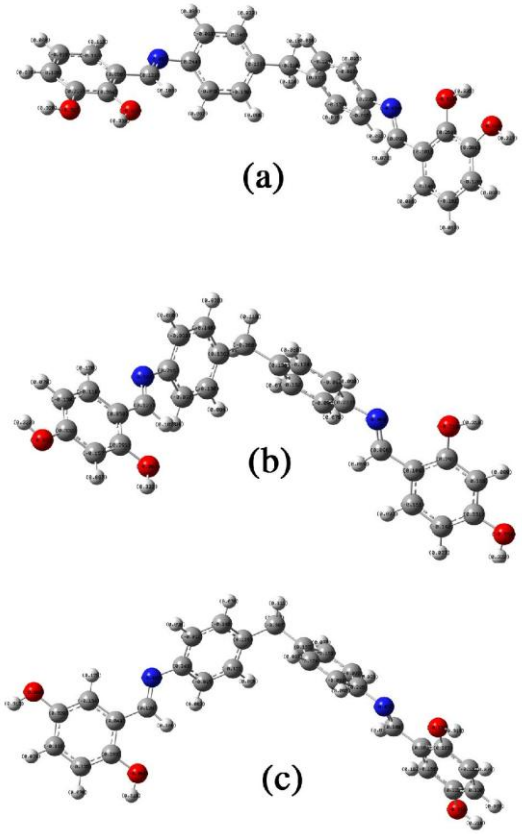

Fig.11. optimized molecular structure, total electron density surface mapped (a) 2,3-DHDPM, (b) 2,4-DHDPM, and (c) 2,5-DHDPM obtained from B3LYP/6-31G** method

Dipole moment is a significant structural parameter expressing the polarity of molecules with their tendency to interact with other molecular entities [44]. However, there is a controversy in the literature on the correlation between μ and IE %. Some authors are favourable to that a low value of dipole moment leads to the accumulation of inhibitor molecules on the metal surface as a consequence of increasing of the inhibition efficiency while others think that high dipole moment enhances the adsorption forces on the metallic surface confering them high inhibition performances [45]. So, the dipole moment data obtained from the present study indicated that 2.5-DHDPM component used as inhibitor has given the highest value of μ, associated to higher inhibition efficiency than those of 2.4-DHDPM and 2.3-DHDPM ligands. The displayed data demonstrate that the values of dipole moment for the studied inhibitor molecules are higher than the dipole moment of water (1.85 Debye). This result suggests that all our inhibitors are endowed with a greater affinity to interact with metal

surface than the water molecules. On this basis, it can be concluded that these inhibitor molecules can adsorb on the MS surface by replacing the water molecules already adsorbed.

The theoretical values of χ and η for Iron were found to be 0 eV and 7 eV, respectively [46]. The values of χ, η, σ and ΔN are shown in Table 4. Several studies [47-48] have denoted that the inhibitor molecule with lower electronegativity (χ) is associated to higher electron donating tendency and therefore, corresponds to a greater inhibitory effect. On the contrary, the hardness (η) measuring the strength towards dislocation of electron cloud of molecules which are disturbed by chemical factors. Thus, hard molecules are characterized by larger values of ΔE which confer less reactivity compared to the soft molecules. Furthermore, the parameter softness (σ) is directly proportional to χ, so a higher σ corresponds to higher efficiency. The value ΔN describes the limit of electron donations. If $\Delta N < 3.6$, the inhibitory efficiency increases with increasing of the ability of the electron donation to the metal surface [49]. The calculated parameters such as gap, softness, hardness, EHOMO and ELUMO show convincingly an excellent correlation with the efficiency of the corrosive inhibition.

2.7 Molecular modeling simulation

In order to explore the favoured adsorption sites privileging the interaction between the considered inhibitors and the carbon steel surface, molecular dynamics were performed in order to determine the possibilities of combination for the investigated molecules and iron surface. As depicted in Table 5, 2.5-DHDPM molecule shows the maximum adsorption energy (-357.63 Kcal/mol) along the simulation operation, among the tested inhibitors 2.3-DHDPM (-356.92 Kcal/mol) and 2.4-DHDPM (-355.67 Kcal/mol) presuming that 2.5-DHDPM inhibitor possesses the higher inhibition efficiency against the corrosion of MS surface. In the case of water environment (600 H_2O) as shown in Fig. 14, presenting the configuration of the inhibitors (2.3-DHDPM, 2.4-DHDPM, 2.5-DHDPM) in the watery phase. The values of Adsorption energy (E_{ads}) seems to be more negative than that obtained in vacuum phase. This proved that the inhibitor is stable in the aqueous phase and strongly binds to the metal surface. Generally, high adsorption Energy corroborates to the more stable chelate between inhibitor and Fe (1 1 0) surface [50].

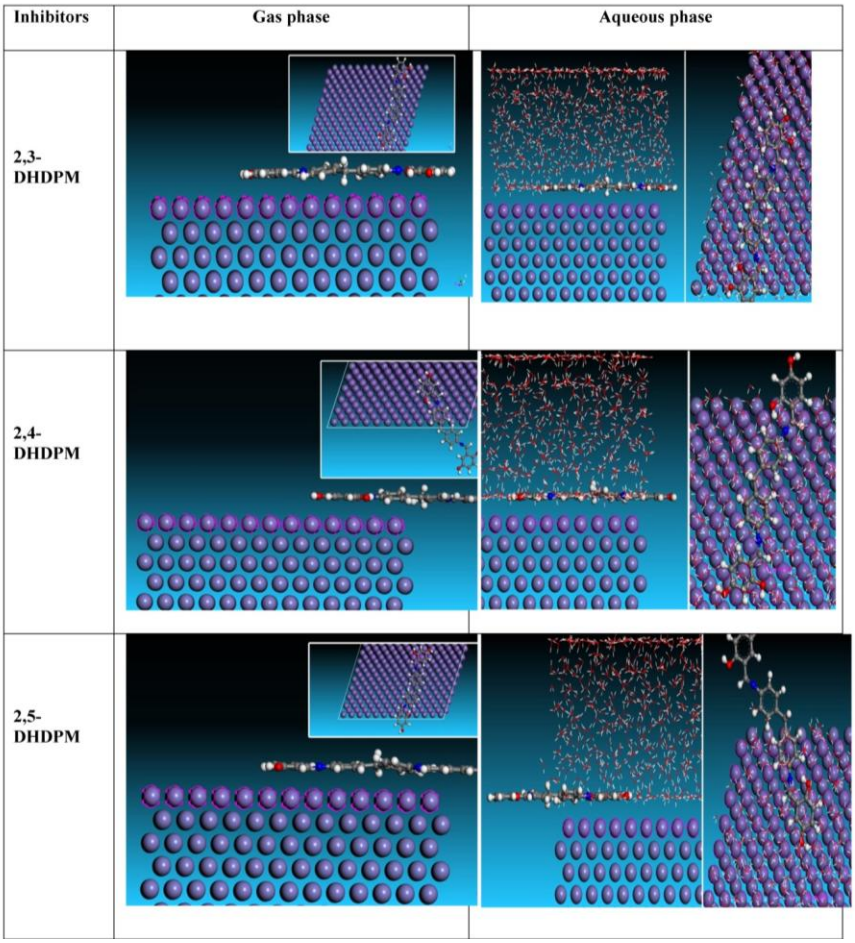

Fig.12. Side views and top views of the most stable configurations for adsorption of, (a) 2,3-DHDPM, (b)2,4-DHDPM, and (c) 2,5-DHDPM on Fe (110) surface calculated using MD simulations in the gas phase and aqueous phase

Table 5. Interaction energies between the inhibitors and Fe (110) surface (kcal/mol)

Inhibitors	Total energy	Adsorption energy	Rigid adsorption energy	Deformation energy	Ead/dNi
(gas phase)					
	-260.14	-353.01	-238.83	-114.17	-353.01
	-306.31	-355.00	-238.96	-116.04	-355.00
	-305.07	-798.31	-239.57	-558.74	-798.31
(aqueous phase)					
	-8156.84	-8156.84	-8596.19	439.35	-13.92
	-8151.91	-8151.91	-8595.07	443.15	-13.15
	-8178.35	-8178.35	-8620.63	442.27	-16.16

The shut interaction between the inhibitor molecules and iron surface as properly as the excellent adsorption configurations for the compounds were illustrated in Fig. 12. The steadiness of the inhibitor molecules and its inhibition effectivity are ordered as 2.5-DHDPM > 2.3-DHDPM > 2.4-DHDPM. These findings are all in suitable accordance with the outcomes acquired from experimental work.

3. EXPERIMENTAL

3.1. Electrodes

Mild steel (MS) named X52 with a composition of (in wt %) C, 0.076; P, 0.012; Si, 0.026; Mn, 0.192; Cr, 0.050; Cu, 0.135; Al, 0.023; Ni, 0.050, and the rest is Fe, was employed as working electrode which was obtained from a cylindrical MS bar of surface area of 0.5 cm2. The sample was polished with emery paper (n^o. 800–1200 grades). The working electrode was degreased with acetone then copiously washed with double-distilled water and lastly dried at room temperature.

3.2. Synthesis of Schiff base compounds

Schiff bases compounds (shown in Fig 1), were synthesized from equimolar amounts of bis-(4-aminophenyl) methane and the corresponding salicylaldehyde via condensation reaction in ethanol [51]. The obtained solid was filtered, washed small portions of cooled ethanol, recrystallized with 50 mL of ethanol and dried under vacuum.

2,3-DHDPM: Melting point (mp) 200 °C; ^{1}H NMR (100 MHz, $CDCl_3$) δ (ppm)= 13.28 (s,2H, C_2OH and C'$_2$OH of 2Ar-OH); 9.17 (s,2H, C_3OH and C'$_3$OH of 2Ar-OH); 8.90 (s, 2H, HC=N); 6.78–7.10 (m, 8H, ArH); 5.20 (2H, s); 4.02 (s, 2H, CH2); FTIR ν (cm^{-1}) 3438 (OH, broad centered at), 1615 (C=N); Microanalysis for $C_{27}H_{22}N_2O_4$ (438.47), Calcd: C, 73.96; H, 5.06; N, 6.39. Found: C, 73.85; H, 5.06; N, 6.39.

2,4-DHDPM: mp 187 °C; ^{1}H NMR (100 MHz, DMSO) δ (ppm)= 13.65 (s,2H, C_2OH and C'$_2$OH of 2Ar-OH), 10.35 (s,2H, C_4OH and C'$_4$OH of 2Ar-OH), 8.75 (s, 2H, HC=N), 6.79–7.38 (m, 8H, ArH), 5.20 (2H, s), 3.96 (s, 2H, CH2); FTIR ν (cm^{-1}) 3400 (OH), 1623 (C=N), 1284 (C–O); Microanalysis for $C_{27}H_{22}N_2O_4$ (438.47), Calcd: C, 73.96; H, 5.06; N, 6.93. Found: C, 73.77; H, 5.06; N,6.42.

2,5-DHDPM: mp 210 °C; ^{1}H NMR (25 MHz, $CDCl_3$) δ (ppm) 12.33 (s,2H, C_2OH and

C'$_2$OH of 2Ar-OH), 9.10 (s,2H, C_5OH and C'$_5$OH of 2Ar-OH), 8.82 (s, 2H, HC=N), 6.80–7.32 (m, 8H, ArH), 5.20 (2H, s), 4.00 (s, 2H, CH2); FTIR ν (cm^{-1}) 3400 (OH), 1620 (C=N); Microanalysis for $C_{27}H_{22}N_2O_4$ (438.47), Calcd: C, 73.96; H, 5.06; N, 6.39. Found: C, 73.81; H, 5.04; N,6.41 .

3.3. Preparation of solutions

The corrosive medium (a solution of 1 M HCl) was obtained by dilution in double-distilled water (Sigma-Aldrich). Because of the low solubility of **2,3-DHDPM**, **2,4-DHDPM** and **2,5-DHDPM** in HCl, the inhibitor was dissolved in 2.5 mL of DMF before addition of 100 mL of 1 M HCl. The various concentrations of the studied inhibitors were 5×10^{-5}M, 10^{-4}M, 5×10^{-4}M and 10^{-3}M.

3.4. Electrochemical measurements

The electrochemical experiments were implemented in a thermostated and double-layered Pyrex cell with a capacity of 150 mL equipped with a conventional device of three electrodes: a platinum electrode (1cm²) as an auxiliary electrode and a saturated calomel electrode (SCE) (Hg/Hg_2Cl_2/KCl) as the reference electrode, the latter was equipped with a Luggin capillary in close proximity to the working electrode to minimize the influence of the Ohmic losses. The electrochemical measurements were performed using a PGSTAT302N autolab and a PC workplace using NOVA software to calculate the resulting electrochemical parameters.

Electrochemical impedance spectroscopy was performed across a range of AC signals (5 mV) from each peak through the open circuit potential in the frequency range of 100 kHz–10 mHz. The immersion time before the measurement was 30 minutes, which proved to be sufficient for corrosion potential E_{corr} to get a reliable value. The curve plots of polarization are potentiodynamic and registered from -600 to -200 mV (vs SCE), with a scanning speed of 0.5 $mV.s^{-1}$. Inhibition efficiency (IE%) was calculated following equation 1.

$$\text{IE }\% = \frac{i_{blank} - i_{inh}}{i_{blank}} \times 100 \qquad (10)$$

Where i_{blank} and i_{inh} are the obtained corrosion current densities without and with inhibitors, respectively. The corrosion current densities were estimated using the Stern-Geary equation:

$$i_{corr} = \frac{1}{2.303R_p} \times \frac{\beta_a \beta_c}{\beta_a + \beta_c} \quad (11)$$

Where βa and βc are the anodic and cathodic Tafel slopes, respectively.

For the determination of the polarization resistance (Rp), the potential of the working electrode was ramped up to ±10 mV near E_{corr} at a scan rate of 0.1 mV $s^{-1.}$

The AC impedance measurements were realized in the frequency gamut started from 100 KHz until 10 mHz at the rest potential, with amplitude of 5 mV. All experiments were achieved under atmospheric conditions.

3.5. Atomic force microscopy studies

The MS surface, after exposure to a 1 M HCl solution in the absence (or presence) of 1 mM of inhibitor for 12 hours, was examined via AFM (MPE 3D model, Asylum Research, Oxford Instruments).

3.6. Scanning electron microscopy (SEM-EDS)

Surface analysis and EDS of the MS coupons was performed in absence and presence of optimum concentrations of Schiff bases (SBs) using a scanning electron microscope MEB-EDX Quanta 250 at 1000-fold higher magnification after immersing them in 1 M HCl for 24 hours.

3.7. Quantum chemical calculations

All the calculations were executed with Gaussian 09W package via DFT method with 6-31G** basis set. [52]. The following quantum parameters were determined: highest occupied molecular orbital energy (E_{HOMO}), lowest unoccupied molecular orbital energy (E_{LUMO}), the E_{HOMO}–E_{LUMO} energy gap (ΔE), global hardness (γ), global softness (σ), electronegativity (χ), the fraction of electrons transferred (ΔN) and Mulliken charges on the backbone atoms [53].

3.8. Molecular modeling simulation

Extinguish MD simulation was performed utilizing Forcite module in the Material Studio Software 7.0 from BIOVIA-Accelrys, USA27, 28. The modelling was achieved on Fe (110) crystal in a 5 A° deep slab using the periodic boundary conditions representative part of an interface that is devoid of any arbitrary boundary effects. The Fe (110) plane was then

expanded to a 13 × 13 supercell to give a suitably substantial surface to the connections of the contemplated inhibitor with the metallic surface. A vacuum slab of 50 Å thickness was later built above the Fe (110) plane and the Fe (110) surface was fixed before the simulations. The entire components of the systems, i.e. Fe (110) + inhibitor were optimized using the Condensed-phase Optimized Molecular Potentials for Atomistic Simulation Studies (COMPASS) force field and aqueous phase. The MD simulations were performed in NVT canonical ensemble at 298 K, a time step of 1.0 fs, and a total simulation time of 500 ps using Anderson thermostat. The MD simulations for the advised inhibitors were elaborated in gas and aqueous phase. 600 water molecules were inserted inside the simulation box to mimic a real corrosive environment. The adsorption energy ($E_{adsorption}$) was calculated using the following equations [54].

$$E_{adsorption}=E_{molecule}+E_{surface}-(E_{molecule}+E_{surface}) \quad (12)$$

where $E_{molecule}$ is the potential energy of the SBs molecules, $E_{surface}$ and $E_{molecule+surface}$ are the potential energy of the metal surface system without and with adsorbing SBs Gemini molecules, respectively.

4. CONCLUSION

Three novel inhibitors like 2,3-DHDPM, 2,4-DHDPM and 2,5-DHDPM) were synthesized and characterized by ^{1}H NMR, FT-IR spectroscopy and elementary analysis. The inhibition behavior of ligands (SBs) against the corrosion of X52 MS in 1 M HCl was elaborated via potentiodynamic and electrochemical impedance techniques that lead to the following conclusions:

- The corrosion of MS in the acidic media is significantly reduced upon the addition of the three tetradentate tested SBs, consequently the inhibition efficiency of inhibitors increased. Also, it was found that 2,5-DHDPM is endowed with the better inhibition effect for corrosion of X52 MS under acidic conditions, which is remarkably adsorbed on the metal surface according to Langmuir adsorption isotherm.

- The azomethine (-N=C<) and phenolic (-C-OH) groups revealed that these compounds induce a moderate effect towards the inhibition efficiency but, when the second hydroxyl is fixed on the para position of the salicylaldehyde with co-planarity of its diverse sp^2 moieties led to the best conformation inducing the inhibition efficiency.
- The quantum chemical computation studies displayed that the inhibition effect increased when the lower ΔE gap values decrease and of dipole moment values increase. Dynamic molecular simulation results reveal that the inhibitors performance pursues the order: 2,5-DHDPM > 2,3-DHDPM > 2,4-DHDPM in vacuum and aqueous phase. MD simulation combined with quantum calculation outcomes well-matched with those obtained experimentally. It is conspicuous that this investigation affirmed the validity uses of these methods which compare different fields of research, such as quantum chemistry approach, MD simulation which issues from classical physics and experimental chemistry. This is consistent also with the thermodynamic parameter ΔG^0_{Ads}, displaying values suggesting that the implicated interactions in this process may occur in both physical and chemical adsorptions.
- Surface analysis proves the protection ability of the SBs molecules on the metal surface, which was demonstrated by SEM and EDX analyses suggesting the generation of a protective film on the MS surface.

5. ACKNOWLEDGEMENTS

The authors would like to thank « Direction Générale de la Recherche Scientifique et du Développement Technologique- Algérie » for the financial support.

6. REFERENCES

[1] Woodard & Curran Inc., Industrial Waste Treatment Handbook, 2006.

[2] E.B. Shone, “Corrosion in the petrochemical industry”; 1995.

[3] S.M.A. Hosseini, A. Azimi, The inhibition of mild steel corrosion in acidic medium by 1-methyl-3-pyridin-2-yl-thiourea, Corros. Sci. 51 (2009) 728–732.

[4] Y. Feng, S. Chen, W. Guo, Y. Zhang, G. Liu, Inhibition of iron corrosion by

5,10,15,20-tetraphenylporphyrin and 5,10,15,20-tetra-(4-chlorophenyl)porphyrin adlayers in 0.5 M H2SO4 solutions, J. Electroanal. Chem. 602 (2007) 115–122.

[5] I. Ahamad, M.A. Quraishi, Bis (benzimidazol-2-yl) disulphide: An efficient water soluble inhibitor for corrosion of mild steel in acid media, Corros. Sci. 51 (2009) 2006–2013.

[6] M.A. Hegazy, A.M. Badawi, S.S. Abd El Rehim, W.M. Kamel, Corrosion inhibition of carbon steel using novel N-(2-(2-mercaptoacetoxy)ethyl)-N,N-dimethyl dodecan-1-aminium bromide during acid pickling, Corros. Sci. 69 (2013) 110–122.

[7] K.R. Ansari, M.A. Quraishi, A. Singh, Schiff's base of pyridyl substituted triazoles as new and effective corrosion inhibitors for mild steel in hydrochloric acid solution, Corros. Sci. 79 (2014) 5–15.

[8] M. Yadav, D. Behera, S. Kumar, P. Yadav, Experimental and Quantum Chemical Studies on Corrosion Inhibition Performance of Thiazolidinedione Derivatives for Mild Steel in Hydrochloric Acid Solution, Chem. Eng. Commun. 202 (2015) 303–315.

[9] M. Hosseini, S.F.L. Mertens, M. Ghorbani, M.R. Arshadi, Asymmetrical Schiff bases as inhibitors of mild steel corrosion in sulphuric acid media, Mater. Chem. Phys. 78 (2003) 800–808.

[10] A. Yurt, S. Ulutas, H. Dal, Electrochemical and theoretical investigation on the corrosion of aluminium in acidic solution containing some Schiff bases, Appl. Surf. Sci. 253 (2006) 919–925.

[11] B. Xu, W. Yang, Y. Liu, X. Yin, W. Gong, Y. Chen, Experimental and theoretical evaluation of two pyridinecarboxaldehyde thiosemicarbazone compounds as corrosion inhibitors for mild steel in hydrochloric acid solution, Corros. Sci. 78 (2014) 260–268.

[12] MEDINA, Juan J. Martínez, NASO, Luciana G., PÉREZ, Ana L. Antioxidant and anticancer effects and bioavailability studies of the flavonoid baicalin and its oxidovanadium (IV) .J. Inorg. Biochem**,** 166 (2017) 150–161

[13] GABER, Mohamed, EL-GHAMRY, Hoda A., FATHALLA, Shaimaa K., *et al.* Synthesis, spectroscopic, thermal and molecular modeling studies of Zn^{2+}, Cd^{2+} and UO_2^{2+} complexes of Schiff bases containing triazole moiety. Antimicrobial, anticancer,

antioxidant and DNA binding studies. Mater. Sci. Eng. C, 83 (2018) 78-89..

[14] WU, Jia-Ning, CHEN, Lin, FU, Teng, et al. New application for aromatic Schiff base: High efficient flame-retardant and anti-dripping action for polyesters. Chem. Eng. J. 336 (2018) 622-632.

[15] T. Zaiz, T. Lanez. Application of some ferrocene derivatives in the field of corrosion inhibition. Journal of Chemical and Pharmaceutical Research, 2012, 4(5):2678-2680.

[16] K. Ramya, R. Mohan, K.K. Anupama, A. Joseph, Electrochemical and theoretical studies on the synergistic interaction and corrosion inhibition of alkyl benzimidazoles and thiosemicarbazide pair on mild steel in hydrochloric acid, Mater. Chem. Phys. VO - 149-150. (2015) 632.

[17] K Toumiat., A Guibadj., M.B Taouti., T.LaneZ. Electrochemical study and computational details of copper corrosion inhibition by 1h-benzotriazole in 3 % wt. NaCl medium, Mor. J. Chem. 2015, 3(2) 809-823.

[18] R. Solmaz, E. Altunbaş and G. Kardaş, Adsorption and corrosion inhibition effect of 2-((5-mercapto-1,3,4-thiadiazol-2-ylimino)methyl)phenol Schiff base on mild steel, Mater. Chem. Phys. 125 (2011) 796-801.

[19] EL-LATEEF, Hany M. Abd, ABU-DIEF, Ahmed M., ABDEL-RAHMAN, Laila H., *et al.* Electrochemical and theoretical quantum approaches on the inhibition of C1018 carbon steel corrosion in acidic medium containing chloride using some newly synthesized phenolic Schiff bases compounds, *J. Electroanal.Chem.* 743 (2015) 120-133.

[20] DANAEE, I., GHASEMI, O., RASHED, G. R., *et al.* Effect of hydroxyl group position on adsorption behavior and corrosion inhibition of hydroxybenzaldehyde Schiff bases: Electrochemical and quantum calculations, J. Mol. Struct. 1035 (2013) 247-259.

[21] Heydari, Hossein, et al. Comparison of two Schiff bases containing O-methyl and nitro substitutes for corrosion inhibiting of mild steel in 1 M HCl solution, J. Molec. Liq 254 (2018) 177-187.

[22] Al-Azawi, Khalida F., et al. Experimental and quantum chemical simulations on the corrosion inhibition of mild steel by 3-((5-(3, 5-dinitrophenyl)-1, 3, 4-thiadiazol-2-yl) imino) indolin-2-one, Results in Physics 9 (2018) 278-283.

[23] Al-Baghdadi, Shaimaa B., et al. Synthesis and corrosion inhibition application of NATN on mild steel surface in acidic media complemented with DFT studies, Results in Physics 8 (2018) 1178-1184.

[24] Kadhim, Abdulhadi, et al. Experimental and theoretical studies of benzoxazines corrosion inhibitors, Results in physics 7 (2017) 4013-4019.

[25] Salarvand, Zohreh, et al. Enhanced corrosion resistance of mild steel in 1 M HCl solution by trace amount of 2-phenyl-benzothiazole derivatives: Experimental, quantum chemical calculations and molecular dynamics (MD) simulation studies, Corr. Sci 114 (2017): 133-145.

[26] Guo, Lei, et al. "Toward understanding the anticorrosive mechanism of some thiourea derivatives for carbon steel corrosion: A combined DFT and molecular dynamics investigation, J. Coll. Interface. sci 506 (2017) 478-485.

[27] Belhadj, N., Ourari, A., Keraghel, S., Schöllhorn, B., & Matt, D. Crystal Structure and Corrosion Inhibition Properties of Ferrocenyl-and Phenylendiamine-Iminomethylphenoxy Cobalt Complexes. J Chem Crystallogr 47.1-2 (2017): 40-46.

[28] L. Toukal, S. Keraghel, F. Benghanem, A. Ourari, Electrochemical, Thermodynamic and Quantum Chemical Studies of Synthesized Benzimidazole Derivative as an ecoFriendly Corrosion Inhibitor for XC52 Steel in Hydrochloric Acid, Int. J. Electrochem. Sci., 13 **(**2018**)** 951 – 974.

[29] S.K. Saha, A. Dutta, P. Ghosh, D. Sukul, P. Banerjee, Adsorption and corrosion inhibition effect of Schiff base molecules on the mild steel surface in 1 M HCl medium: a combined experimental and theoretical approach, Phys. Chem. Chem. Phys. 17 (2015) 5679–5690.

[30] B. El Mehdi, B. Mernari, M. Traisnel, F. Bentiss, M. Lagrenée, Synthesis and comparative study of the inhibitive effect of some new triazole derivatives towards corrosion of mild steel in hydrochloric acid solution, Mater. Chem. Phys. 77 (2003) 489–496.

[31] E. a. Noor, A.H. Al-Moubaraki, Thermodynamic study of metal corrosion and inhibitor

adsorption processes in mild steel/1-methyl-4[4???(-X)-styryl pyridinium iodides/hydrochloric acid systems, Mater. Chem. Phys. 110 (2008) 145–154.

[32] X. Li, S. Deng, H. Fu, Inhibition of the corrosion of steel in HCl, H2SO4 solutions by bamboo leaf extract, Corros. Sci. 62 (2012) 163–175.

[33] A.A. Gü Rten, H. Lya Keles, E. Bayol, F. Kandemirli, The effect of temperature and concentration on the inhibition of acid corrosion of carbon steel by newly synthesized Schiff base, J. Ind. Eng. Chem. 27 (2015) 68–78.

[34] Z. El Adnani, M. Mcharfi, M. Sfaira, M. Benzakour, A.T. Benjelloun, M. Ebn Touhami, DFT theoretical study of 7-R-3methylquinoxalin-2(1H)-thiones (RH; CH3; Cl) as corrosion inhibitors in hydrochloric acid, Corros. Sci. 68 (2013) 223–230.

[35] H. Ju, Z.P. Kai, Y. Li, Aminic nitrogen-bearing polydentate Schiff base compounds as corrosion inhibitors for iron in acidic media: A quantum chemical calculation, Corros. Sci. 50 (2008) 865–871.

[36] S. Xia, M. Qiu, L. Yu, F. Liu, H. Zhao, Molecular dynamics and density functional theory study on relationship between structure of imidazoline derivatives and inhibition performance, Corros. Sci. 50 (2008) 2021–2029.

[37] R.G. Pearson, Absolute electronegativity and hardness: application to inorganic chemistry, Inorg. Chem. 27 (1988) 734–740.

[38] R. Yıldız, An electrochemical and theoretical evaluation of 4,6-diamino-2-yrimidinethiol as a corrosion inhibitor for mild steel in HCl solutions, Corros. Sci. 90 (2015) 544–553.

[39] M. Yadav, S. Kumar, N. Kumari, I. Bahadur, E.E. Ebenso, Experimental and Theoretical Studies on Corrosion Inhibition Effect of Synthesized Benzothiazole Derivatives on Mild Steel in 15% HCl Solution, Int. J. Electrochem. Sci. Int. J. Electrochem. Sci. 10 (2015) 602–624.

[40] Xia S, Qiu M, Yu L, Liu F, Zhao H. Molecular dynamics and density functional theory study on relationship between structure of imidazoline derivatives and inhibition performance. Corros Sci. 50 (2008) 2021–2029.

[41] Musa AY, Kadhum AH, Mohamad AB, Rahoma AB, Mesmari H. Electrochemical and

quantum chemical calculations on 4,4-dimethyloxazolidine-2-thione as inhibitor for mild steel corrosion in hydrochloric acid. J Mol Struct. 969 (2010) 233–237.

[42] Verma C., Quraishi M. A. & Singh A. 2-Aminobenzene-1, 3-dicarbonitriles as green corrosion inhibitor for mild steel in 1 M HCl: Electrochemical, thermodynamic, surface and quantum chemical investigation. J. Taiwan Ins. Chem. Eng. 49 (2015) 229–239

[43] I. Ahamad, R. Prasad, M.A. Quraishi, Thermodynamic, electrochemical and quantum chemical investigation of some Schiff bases as corrosion inhibitors for mild steel in hydrochloric acid solutions, Corros. Sci. 52 (2010) 933–942.

[44] G. Gece, The use of quantum chemical methods in corrosion inhibitor studies, Corros. Sci. 50 (2008) 2981–2992.

[45] A. Ongun Yüce, B. Doğru Mert, G. Kardaş, B. Yazıcı, Electrochemical and quantum hemical studies of 2-amino-4-methyl-thiazole as corrosion inhibitor for mild steel in HCl solution, Corros. Sci. 83 (2014) 310–316.

[46] M. Shahraki, M. Dehdab, S. Elmi, Theoretical studies on the corrosion inhibition performance of three amine derivatives on carbon steel: molecular dynamics simulation and density functional theory approaches, Taiwan Inst. Chem. Eng. 62 (2016) 313-321.

[47] Singh, A., Ansari, K. R., Haque, J., Dohare, P., Lgaz, H., Salghi, R., & Quraishi, M. A, Effect of electron donating functional groups on corrosion inhibition of mild in hydrochloric acid: Experimental and quantum chemical study, Taiwan Inst. Chem. Eng., 82 (2018) 233-251.

[48] Ankush Mishra , Chandrabhan Verma , H. Lgaz , Vandana Srivastava , M.A. Quraishi , Eno E. Ebenso. Synthesis, characterization and corrosion inhibition studies of *N*-phenyl-benzamides on the acidic corrosion of mild steel: Experimental and computational studies, J. mol. liq. 251 (2018) 317–332.

[49] Musa, Ahmed Y., Ramzi TT Jalgham, and Abu Bakar Mohamad. "Molecular dynamic and quantum chemical calculations for phthalazine derivatives as corrosion inhibitors of mild steel in 1 M HCl, Corr. Sci 56 (2012) 176-183

[50] Elemike, Elias E., et al. Synthesis, crystal structures, quantum chemical studies and corrosion inhibition potentials of 4-(((4-ethylphenyl) imino) methyl) phenol and

(E)-4-((naphthalen-2-ylimino) methyl) phenol Schiff bases, J. Molec. Struct 1147 (2017) 252-265.

[51] M. Salavati-Niasari, M. Bazarganipour, Effect of single-wall carbon nanotubes on direct epoxidation of cyclohexene catalyzed by new derivatives of cis-dioxomolybdenum(VI) complexes with bis-bidentate Schiff-base containing aromatic nitrogen-nitrogen linkers, J. Mol. Catal. A Chem. 278 (2007) 173–180.

[52] M. J. Frisch, G. W. Trucks, H. B. Schlegel, G. E. Scuseria, M. A. Robb, J. R. Cheeseman, G. Scalmani, V. Barone, B. Mennucci, G. A. Petersson, H. Nakatsuji, M. Caricato, X. Li, H. P. Hratchian, A. F. Izmaylov, J. Bloino, G. Zheng, J. L. Sonnenberg, M. Hada, M. Ehara, K. Toyota, R. Fukuda, J. Hasegawa, M. Ishida, T. Nakajima, Y. Honda, O. Kitao, H. Nakai, T. Vreven, J. A. Montgomery, Jr., J. E. Peralta, F. Ogliaro, M. Bearpark, J. J. Heyd, E. Brothers, K. N. Kudin, V. N. Staroverov, R. Kobayashi, J. Normand, K. Raghavachari, A. Rendell, J. C. Burant, S. S. Iyengar, J. Tomasi, M. Cossi, N. Rega, J. M. Millam, M. Klene, J. E. Knox, J. B. Cross, V. Bakken, C. Adamo, J. Jaramillo, R. Gomperts, R. E. Stratmann, O. Yazyev, A. J. Austin, R. Cammi, C. Pomelli, J. W. Ochterski, R. L. Martin, K. Morokuma, V. G. Zakrzewski, G. A. Voth, P. Salvador, J. J. Dannenberg, S. Dapprich, A. D. Daniels, Ö. Farkas, J. B. Foresman, J. V. Ortiz, J. Cioslowski, and D. J. Fox, Gaussian 09, Revision D.01, Gaussian, Inc., Wallingford CT, 2009.

[53] S. Xia, M. Qui, L. Yu, F. Lui, H. Zhao, “Molecular dynamics and density function theory study on relationship between structure of imidazoline derivatives and inhibition performance, Corros. Sci. 50 (2008) 2012–2029.

[54] H. Keleş, M. Keleş, I. Dehri, O. Serindağ, Adsorption and inhibitive properties of aminobiphenyl and its Schiff base on mild steel corrosion in 0.5 M HCl medium, Colloids Surfaces A Physicochem. Eng. Asp. 320 (2008) 138–145.

How to cite this article:
Kheniche A, Ourari A, Dakhouche A, Ghanem A, Min W, Meguellati K. Electrochemical and theoretical studies influencing the effect of hydroxyl position of tetraphenolic schiff bases towards corrosion inhibition of mild steel in 1M HCl. J. Fundam. Appl. Sci., 2018, *10(3), 209-238.*